ROYAL SOCIETY OF CHEMISTRY

PAPER

Check for updates

Sustainable food packaging using modified kombucha-derived bacterial cellulose nanofillers in biodegradable polymers†

Mikhail Koreshkov, [ID] *[a] Yuuki Takatsuna, [ID] [a] Alexander Bismarck, [ID] [b] Ines Fritz, [ID] [c] Erik Reimhult [ID] [a] and Ronald Zirbs [ID] *[a]

Incorporating nanoscale filler materials into polymers usually enhances mechanical properties, alters barrier characteristics, and enhances the visual appeal of consumer polymers. The growing recognition of the imperative to shift away from fossil-based, non-biodegradable polymers in single-use plastics and packaging materials toward fully renewable, recyclable, and/or biodegradable alternatives like PLA or PHBV has underscored the urgent need for the development of new, cost-effective, and scalable filler materials. Here, we demonstrate that the utilization of simple oligo-lactic acid modified bacterial cellulose (OLLA-g-BC) enhances the overall properties of commercial PLA and PHBV to a degree where it can directly compete with established conventional food packaging polymers. The key factor driving this enhancement lies in the uniform dispersion of the nanofiller throughout the bulk polymer, as visualized and confirmed through innovative 3D serial block face SEM analysis. The addition of 5% OLLA-g-BC increased the biodegradation rate of the nanocomposites without compromising their mechanical performance, leading to a ~12% increase in Young's modulus for PLLA and a ~14% decrease for PHBV. Filler incorporation resulted in a ~23% and ~45% decrease in oxygen permeability for PLLA and PHBV, respectively, while a ~12% increase in water vapor permeability was observed for PLLA. Intensive investigations into the performance of nanocomposites clearly indicate that OLLA-grafted bacterial cellulose compound materials could significantly contribute to the realization of a fully circular, zero-waste economy.

Sustainability spotlight

Humanity's ever-increasing demand for single-use plastics poses a significant threat to the natural world. Our research presents an economically viable method to create biodegradable alternatives using cellulose-reinforced industrial nanocomposites derived from agricultural waste. We believe that the technology described is capable of moving the entire field of polymer packaging in a more sustainable direction. This article describes for the first time a simple, cheap and environmentally friendly way to overcome most of the problems encountered when using cellulose as a filler, and not only suggests new ways to use it, but also discusses why this material/approach is worth developing further. Bacterial cellulose, derived from the fermentation of agricultural waste, represents an innovative solution for the production of composites in the manufacturing sector, meeting UN SDGs 9 and 12 and reducing the solid waste. Our goal is to produce biodegradable composites with improved performance that can be integrated into the environment, meeting UN SDGs 14 and 15. Our work contributes to the circular economy by using renewable resources and provide a solution for sustainable food packaging.

[a]Department of Bionanosciences, Institute of Biologically Inspired Materials, University of Natural Resources and Life Sciences (BOKU), Vienna, Austria. E-mail: mikhail.koreshkov@boku.ac.at; ronald.zirbs@boku.ac.at

[b]Polymer and Composite Engineering (PaCE) Group, Institute of Material Chemistry and Research, Faculty of Chemistry, University of Vienna, Vienna, Austria

[c]Department of Agrobiotechnology, Institute of Environmental Biotechnology, University of Natural Resources and Life Sciences (BOKU), IFA-Tulln, Tulln, Austria

Introduction

Moving away from fossil fuel-based polymers, especially in food and beverage packaging, is essential for a sustainable future. Rising plastic consumption, largely from single-use packaging, is increasing CO_2 emissions and exacerbating (micro)plastic pollution, which is having a devastating impact on ecosystems worldwide.[1–3] With packaging accounting for 31% of plastic production, most of which is derived from fossil fuels,[4,5] there is an urgent need for action. Current recycling efforts are hampered by contamination with food waste, resulting in large amounts of plastic waste.[6] Replacing fossil-based polymers with

renewable alternatives, especially biodegradable and/or recyclable polymers such as polylactic acid (PLA) and poly(3-hydroxybutyrate-co-3-hydroxyvalerate) (PHBV), is promising.[7–9] These renewable resources offer environmentally friendly options that align with sustainability goals and minimize ecological damage.[10,11]

State-of-the-art scientific advancements provide a promising approach to tackle challenges associated with renewable and biodegradable polymers in food packaging. Innovative modifications, including the incorporation of nanofiller materials, enhance biodegradable polymers to meet precise requirements while surmounting obstacles such as cost, mechanical limitations, gas barrier inefficiencies, and narrow processing windows.[12–14] Green nanocomposites are instrumental in this enhancement by ameliorating mechanical, thermal, and barrier properties, and accelerating biodegradation rates.[15–17] Effective dispersion and favourable interaction between nanofiller and polymer matrix are essential for optimal composite performance.[18,19]

Cellulose fillers have emerged as a potential avenue for green composites;[20,21] however, their reinforcing effectiveness is often hampered by uneven distribution, especially during industrial polymer processing methods.[22,23] Insufficient data exists regarding the dispersion state of cellulose-based fillers due to low contrast with the polymer matrix, thermal sensitivity, and limitations in sample analysis techniques. Current characterization methods primarily focus on surface distribution, potentially misrepresenting the overall 3D dispersion.

Utilizing nanocellulose, reduced to nano-scale dimensions, enhances dispersibility and boosts the interfacial area between the polymer matrix and cellulose reinforcement.[14] However, hydrophilic cellulose nanoparticles struggle to uniformly disperse in hydrophobic polymer matrices, leading to clustering and decreased mechanical and barrier properties in renewable polymer composites like poly-L-lactic acid (PLLA) and PHBV.[24] Research focuses on reducing interfacial energy between cellulose nanoparticles and hydrophobic biodegradable polymer matrix, primarily through chemical surface modifications.[14,25] Grafting polymer chains onto nanocellulose surfaces shows promise, initiating polymerization of matrix-compatible polymers from cellulose sites[26] to create a cellulose core with a grafted polymer shell, enhancing dispersion of filler within the polymer matrix.

Wood pulp is a common source of nanocellulose; however, extracting nanocellulose from plant matrices, where cellulose intertwines with other biopolymers like lignin, pectin, and hemicellulose, proves uneconomical for applications such as food packaging due to high energy and chemical requirements.[27,28] Bacterial cellulose (BC) emerges as a promising alternative due to its natural abundance, high crystallinity, and the ease of forming BC nanoparticles, devoid of other biopolymers present in wood pulp.[29–32] While BC is currently produced in limited quantities and is relatively expensive,[28,33] emerging circular economy practices utilize millions of tons of food waste, including fruit waste directly sourced from farms, to produce various products with the aim of achieving zero waste, including BC as a viable option.[34–36]

Many proposed methods in literature for modifying cellulose with biodegradable polymers involve unstable intermediates and prove complex, making upscaling impractical.[37,38] Studies predominantly focus on grafting polymer brushes onto micro- and nanocrystalline cellulose,[24,39] demanding higher energy inputs than intrinsically nanoscale BC production. Limited investigations exist on modifying nanosized BC with biodegradable polymers like PLLA. Moreover, the industrial applicability of methods explored is hindered by reliance on solvent casting in most of the existing studies, which lacks potential for industrial implementation.[40,41]

We present a simple and scalable process for the production of BC nanoparticles from kombucha and its grafting with oligo-L-lactic acid (OLLA) (Fig. 1). The integration of these composites into renewable and biodegradable polymer matrices enhances the biodegradability and barrier properties of PLLA and PHBV, making them suitable for food packaging applications. Using conventional polymer processing methods such as extrusion, compression and injection molding, nanocomposites were produced. These nanocellulose green nanocomposites were investigated using advanced 3D block surface SEM, which highlights the importance of surface functionalization of the filler by visualizing and quantifying the nanoscale dispersion achieved in the polymer blend. Our comprehensive evaluation included mechanical properties, gas permeability and biodegradation rate, highlighting the central role of nanoscale dispersion in creating environmentally friendly nanocomposites for sustainable food packaging industry.

Nano-filler materials frequently prompt discussions regarding food safety and end-of-life considerations, such as microplastics. The cellulose-OLLA nanofiller described in this study exhibits safety in all known aspects. Cellulose particles, abundant in nature, are fully biodegradable and extensively researched, while PLA itself is approved by major food and health organizations including the FDA and European regulatory bodies. These investigations aim to demonstrate the potential of current methods and the utilization of economically viable bio-based, biodegradable, and fully recyclable
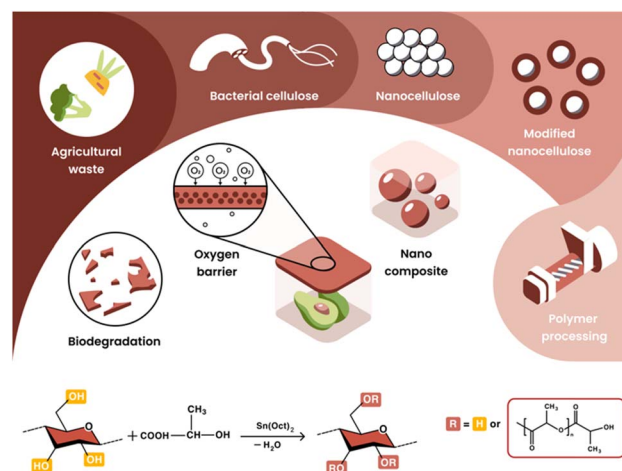

Fig. 1 Representation of the concept explored in this paper.

polymers (such as PLA) to demonstrate the feasibility of green nanocomposites as potential alternatives for food packaging materials. This paves the way for the complete substitution of fossil-based, non-biodegradable, and largely non-recyclable conventional polymers with sustainable alternatives.

Experimental

Materials

PLLA was purchased from Biomer (L9000, MW $\geq$ 150 kg mol^{-1}, D-content 1.5%). PHBV was purchased from Tianan Biological Materials (ENMAT Y1000P, HV content 3%, injection molding grade, with <0.5% boron nitride as nucleating agent and about 1% antioxidant Irganox 1010). 1,4-Dioxane and chloroform (Sigma-Aldrich, $\geq$99% purity) were used as the solvents for PLLA and PHBV respectively. Lactic acid (Aldrich, solute concentration: 85 wt%), sodium hydroxide (Aldrich, pellets, $\geq$98% purity), tin(II) 2-ethylhexanoate (Sn(Oct)$_2$, Aldrich, $\geq$85% purity), dichloromethane and alcohol were purchased from Sigma-Aldrich. The raw bacterial cellulose material was SCOBY, a by-product of fermentation during kombucha production.

SCOBY production

100 mL of fully fermented kombucha tea (sucrose content <5%) and approximately 10v% of previously produced SCOBY were mixed with 10 g L^{-1} of agricultural waste obtained after boiling of leaves and mixed biowaste for 10 min. The fermentation was carried out for 15 d at RT, resulting in SCOBY production.

BC extraction from SCOBY

The extraction and purification of BC from SCOBY was performed as follows:[14] BC was extracted from 800 g of SCOBY, which was blended for 1 min using a laboratory blender. The blended BC was homogenized at 25 000 rpm in 3 L of distilled water for 2 min using a homogenizer (IKA T18 basic ULTRA TURRAX, Staufen, Germany), centrifuged to remove excess water and re-dispersed in 0.1 M NaOH solution at 80 °C for 20 min. The purified BC was washed to neutral pH and freeze dried.

Introduction of lactic acid into the inside of BC

Experimental design for the introduction of lactic acid into the inside of BC and the synthesis of OLLA-g-BC was developed by optimizing the procedures previously reported for microcrystalline cellulose.[32,39,42] 4 g of dry BC was added to 107.6 mL of water at room temperature and homogenized at 25 000 rpm using a homogenizer (IKA T18 basic ULTRA TURRAX, Staufen, Germany). 10 g of NaOH was dissolved in the mixture, which was then frozen at −24 °C for 48 h. Then the flask with tight solid mass was transferred from the freezer to room temperature to thaw, and 82.4 mL water was added followed by mechanical homogenization of the thawing mixture to produce the suspension of solubilized and size-reduced BC. The partial disruption of the hydrogen bonds between the nanofibrils increased the accessibility of the OH groups. BC fibrils were subjected to solvent exchange with 250 mL of lactic acid (LA).

The resulting mixture was centrifuged, washed with LA one more time and freeze dried.

Synthesis of OLLA-g-BC

The reaction mixture (BC/LA = 1/50 wt%) was transferred to the three-neck flask equipped with a mechanical stirrer (Lab Mixer Overhead Stirrer PWR CV S1, IKA Werke, Germany) and a temperature controller. The reaction mixture under vacuum was heated to 120 °C for 2 h. After 1.6 mL Sn(Oct)$_2$ was added and stirred for 30 min under N$_2$ atmosphere. The pressure was then reduced to 20 mbar and polymerisation was carried out by increasing the temperature: 130 °C for 2 h, 140 °C for 2 h, 150 °C for 2 h and 160 °C for 4 h. After the reaction was finished, the mixture was dissolved in dichloromethane and centrifuged. Thereafter, ethanol was added. The precipitate was washed with dichloromethane 4 times and freeze-dried.

Preparation of nanocomposites

3 g of OLLA-g-BC was premixed with 57 g of PLLA and PHBV in 700 mL of dioxane and chloroform, respectively, which were subsequently freeze-dried. Prior to extrusion, both premixed composites were ground in a blender (Nutri-Blender MAX Hochleistungsmixer 2000W, Munich, Germany). The composites with OLLA-g-BC (5 wt%) were fed into a twin-screw microextruder (5 cm^3, Xplore MC 5, Xplore Instruments B.V., Netherlands) and kept in a closed loop for 2 min at 180 °C and screw rotational speed of 100 rpm. The extrudates were compression molded into films using a hot press (George E Moore and Sons, Birmingham, UK) at 180 °C and a pressure of 7.6 MPa for 2 min. The dumbbell-shaped tensile specimens were produced using an injection molding system (HAAKE MiniJet, Thermo Scientific, Netherlands) and a mold (557-2298, ISO 527- 2-5A)[43] with a barrel temperature of 180 °C and a mold temperature of 45 °C.

Methods/characterization

Serial block face (SBF) SEM. The fragments of nanocomposite films were trimmed with a glass knife on a UC-7 ultramicrotome (Leica Microsystems, Vienna, Austria) to 500 μm × 500 μm × 500 μm, coated with a 10 nm gold layer in an EM SCD005 sputter coater (Leica Microsystems) and mounted on the microtome of the Apreo SEM (Thermo Fisher Scientific, Netherlands). Scans were acquired at 1.18 kV, 100 pA, and 3 μs dwell time. The resulting stacks were processed in ImageJ software. Calculations of filler volume fraction and particle size as well as 3D reconstruction were performed in Amira software.

NMR. ^{1}H NMR spectra were recorded on a Bruker AV III 300 MHz spectrometer (BrukerCompany, Switzerland) in dimethyl sulfoxide-d_6 (DMSO-d_6) solvent. The samples were measured at 25 °C and a solute concentration of 6 mg mL^{-1}. The sample was dispersed in DMSO-d_6 and sonicated in an ultrasonic bath for 5 minutes. The calculations of the molar substitution (MS), the degree of lactyl substitution (DS), the average degree of polymerisation of a OLLA side chain (DP), and the mass fraction of OLLA (W$_{OLLA}$) are the averages of at least three measurements.

TEM. Transmission electron microscopy (TEM) images were recorded with an FEI Tecnai G2 (FEI Europe B.V., Austria) with

160 kV acceleration voltage. BC and OLLA-g-BC samples were dispersed in Milli-Q water and DMSO, respectively, sonicated for 10 minutes, and dried on carbon grids under ambient conditions.

Dynamic light scattering (DLS). The modified and regenerated BC were dispersed in DMSO and lactic acid, respectively, and sonicated for 10 minutes. Then DLS measurement was carried out on a Malvern Zetasizer Nano-ZS dynamic light scattering device (Malvern Panalytical Ltd, Malvern, UK). The concentration of particles in DMSO and lactic acid was 1 mg mL^{-1}, and the measurements were performed at 25 °C and at least three times.

Thermogravimetric analysis (TGA). TGA was performed on a Mettler Toledo TGA/DSC (Mettler Toledo GmbH, Vienna, Austria) (80 mL min^{-1} nitrogen). The measurement was carried out in a temperature range from 25 to 650 °C with a heating rate of 10 °C min^{-1}. The calculations of W_{OLLA} are the average of at least five measurements.

FTIR. The molecular structures were confirmed by Fourier Transform Infrared Spectroscopy (FT-IR) using a FT-IR ATR spectrometer (Vertex 70, Bruker Austria GmbH, Vienna, Austria), 32 scans at the wavelength range of 650–4000 cm^{-1} in the transmission mode. Substances were directly mounted on the ATR unit and measured with the pressure stamp.

Mechanical test. Tensile tests were performed following ASTM D638 (ref. 44) using a universal dual column testing frame (Series 5969, Instron Ltd., Norwood, UK). The strain was recorded using a video extensometer (IMT-CAMO018, camera: GigE PoE, IMETRUM, UK) tracking black dots, which were painted on "dog-bone" specimens using opaque black permanent marker. The testing rate was 0.5 mm min^{-1}. At least five replicates were tested for each material and Student's t-test was used to examine the statistical significance of the difference between the pure polymers (PLLA or PHBV) and their respective composites.

Oxygen transmission rate. The oxygen transmission rate (OTR) was measured in a gas permeability tester (VAC-VBS, Labthink Instruments Co. Ltd., China) according to the standard GB/T1038-2000.[45] The tested area was a circular shape with a diameter of 80 mm. The test was performed using a proportional mode with a 10% pressure difference. Prior to the test, the specimens were conditioned in the machine for 4 h under vacuum. At least five replicates were tested for each material and Student's t-test was used to examine the statistical significance of the difference between the pure polymers (PLLA or PHBV) and their respective composites.

Water vapor transmission rate. Water vapor transmission rate (WVTR) was recorded using a WVTR Tester W3/031 (Labthink Instruments Co., China) according to the standard GB/T 1037-1988.[46] The relative humidity (RH) was fixed to 100% in the wet chamber and 10% in the dry chamber, yielding a driving force of 90% RH. The film of 33.18 cm^2 area was analyzed at the atmospheric pressure and at a temperature of 38 °C. WVTR was determined gravimetrically by weighing the dishes with films every 90 min for 10 cycles. At least five replicates were tested for each material and Student's t-test was used to examine the

statistical significance of the difference between the pure polymers (PLLA or PHBV) and their respective composites.

Biodegradation tests. A four-stage research scheme was implemented according to the standard EN 13432 (ref. 47) and OECD 301B[48] (modified Sturm test). The test volume included 400 mL, 10 mL of mixed bacterial inoculum, and the test substance equivalent to *ca.* 0.3 to 0.6 g of carbon. Each test setup consisted of a blanc, a reference substance and test substances in threefold replicates. The carbon content was determined by element analysis with the photo-oxidation principle. For additional detailed information, please refer to the ESI.†

Results and discussion

Synthesis, chemical and structural characterization of L-lactic acid-grafted bacterial cellulose

The process described in this study was optimized to fundamentally investigate the role of pure OLLA-grafted BC synthesized from kombucha-derived BC, which represents a promising biomaterial for high-performance sustainable applications.[49] This fundamental study aimed to characterize the properties of the pure OLLA-g-BC filler, which required the implementation of a purification process to remove any free PLA generated during synthesis. For this purpose, dichloromethane, a well-known solvent for PLA that is easily recyclable but neither biobased nor harmless, was used. It is also important to note that for industrial applications, this purification step is not necessary, allowing for the avoidance of dichloromethane.

The preparation of OLLA-grafted nanocellulose was qualified by FTIR and quantified by NMR and TGA by comparing OLLA-g-BC to BC, OLLA and PLLA. ATR-FTIR spectra of these compounds are presented in Fig. 2A. The IR spectrum of OLLA-g-BC showed the characteristic PLLA bands at 1750, 1450, and 1200 cm^{-1}, which were assigned to C=O stretching mode, methyl asymmetric deformation, and symmetric C–O–C stretching modes of the ester, respectively.[50] The characteristic BC band at 890 cm^{-1} was observed, corresponding to C–O–C stretching in the β-glycosidic linkage.[51]

The structure of the OLLA-g-BC was determined by ^{1}H-NMR (Fig. 2D). By comparing the peak area of denoted peaks in Fig. 2C, we calculated the degree of lactyl substitution (DS$_{OLLA}$), representing the average number of hydroxyl groups per anhydroglucose repeating unit substituted by OLLA using eqn (1), the degree of polymerization of the OLLA side chains (DP$_{OLLA}$) and the average number of lactyl units per anhydroglucose repeating unit (MS$_{OLLA}$) using eqn (2) and (3). The mass fraction of OLLA in the sample (W$_{OLLA}$) was estimated using the molecular weights of 162 g mol^{-1} for anhydroglucose (MW$_{AGU}$) and 72 g mol^{-1} for lactyl (MW$_{lactyl}$) by eqn (4).

$$DS_{OLLA} = \frac{I_D/3}{I_E + I_D/3} \times 3 \tag{1}$$

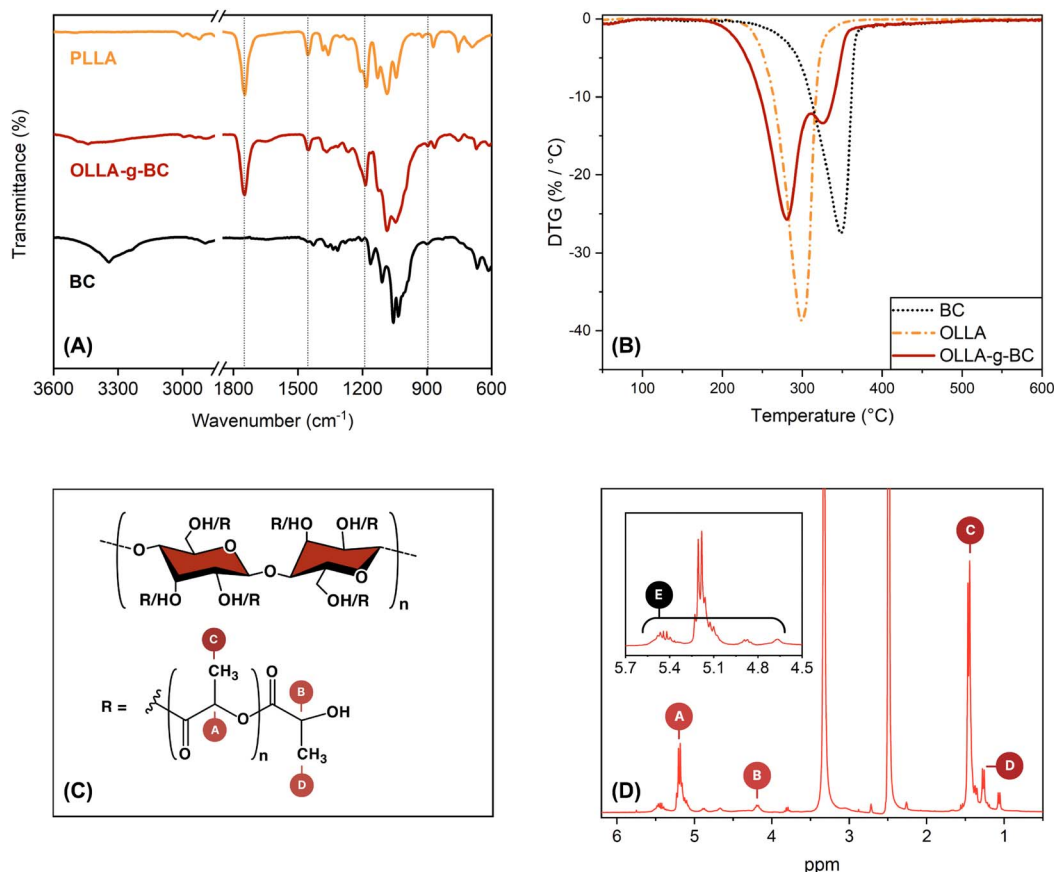$$DP_{OLLA} = \frac{I_D + I_C}{I_D} \tag{2}$$

Fig. 2 Analytics of OLLA grafted BC; (A) FTIR spectra of OLLA-g-BC, BC, and PLLA, showing the successful grafting of OLLA to BC nanoparticles. (B) Derivative thermogravimetry data for BC, OLLA, and OLLA-g-BC. (C) Chemical structure of OLLA-g-BC marking the allocation of the NMR peaks in (D) ^{1}H-NMR spectra of OLLA-g-BC.

$$MS_{OLLA} = DP_{OLLA} \times DS_{OLLA} \qquad (3)$$

$$W_{OLLA} = \frac{MW_{lactyl} \times MS_{OLLA}}{MW_{AGU} - DS_{OLLA} \times MW_H + MW_{lactyl} \times MS_{OLLA}} \qquad (4)$$

This resulted in $DP_{OLLA} = 6 \pm 1.2$, $DS_{OLLA} = 1.4 \pm 0.2$, $MS_{OLLA} = 8 \pm 1.7$ and $W_{OLLA} = 77 \pm 4.3\%$. The observed DP correlates with previous studies, whereas the DS and MS are higher than that reported for the microcrystalline cellulose-*graft*-poly(L-lactide) produced by melt polycondensation of LA catalysed by Sn^{2+}.[39,51]

The DTG curves for OLLA-g-BC (Fig. 2B) exhibited two distinct peaks, indicating that the thermal degradation of the sample proceeded in two steps. We attributed the low-temperature peak to the decomposition of the OLLA chains grafted to BC and the high-temperature peak to the BC. The decomposition temperatures roughly coincide with those of the pure substances and literature values[52,53] but they are shifted to lower temperatures for the core–shell nanocellulose. Fitting the DTG spectra with two Gaussian functions assuming a linear background over the temperature range of the fit and integrating the areas of the respective Gaussians resulted in an estimate of the OLLA mass fraction of 68 ± 2.9 wt%.

Size and morphology of OLLA-grafted bacterial cellulose

We used dynamic light scattering (DLS) and transmission electron microscopy (TEM) to quantify the size of OLLA-g-BC particles. Fig. 3A shows the number-weighted size distribution of OLLA-g-BC forming stable dispersions in DMSO. In contrast, unmodified BC aggregated and precipitated in DMSO; therefore, the measurements on unmodified BC were performed in LA and revealed that the generated BC consisted of nanoscale particles with a diameter of 66 ± 10 nm and aggregates of 1.4 ± 0.4 μm in size. The OLLA-grafted core–shell particles were predominantly nanoscale with 50 ± 10 nm in diameter. Aggregates or particles larger than 100 nm nonetheless comprised ~92% of the particle volume (Fig. S8†).

An analysis of 97 seemingly quasi-cylindrical and round-shaped particles using TEM, exemplified in Fig. 3(B)–(D), yielded diameters of 76 ± 32 nm, which is consistent with the DLS size distribution for the generated BC and OLLA-g-BC particles. The observed size range and morphologies correlate with the diameter of BC nanofibers[30,54,55] and concur with previous studies, where nanocellulose was treated with aqueous NaOH solutions.[32,42]

Aggregates with collapsed diameters between 98 and 345 nm for OLLA-g-BC and between 365 nm and 1675 nm for generated BC were observed on the TEM grids (Fig. 3B and D). The
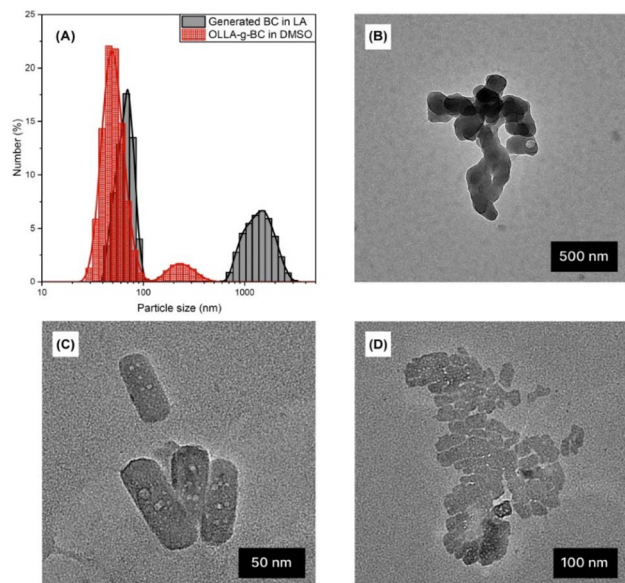
Fig. 3 Size determination of BC and PLLA grafted BC: (A) number-weighted size distributions measured by DLS for OLLA-g-BC in DMSO and regenerated BC in LA. (B) TEM micrographs of aggregates of regenerated BC nanoparticles, (C) quasi-cylindrical OLLA-g-BC nanoparticles, (D) aggregates of OLLA-g-BC nanoparticles.

aggregates sizes observed on the grids only correlated weakly with the dimensions and fractions measured by DLS; this is expected as aggregates are mainly formed on the grid due to drying effects. The formation of aggregates by drying of suspensions that contained individually dispersed particles is also indicated by the apparent gaps between individual OLLA-g-BC particles arranged in 2D (Fig. 3D), which indicate the OLLA shell.

Polymer/L-lactic acid-grafted bacterial cellulose nanocomposites

We chose a filler loading of 5 wt%, at or above the high end of filler concentrations that are typically used in nanocellulose composites.[15,56] We hypothesized that the core–shell nature will improve the interfacial compatibility between nanofiller and polymer matrix and dispersibility, which would allow us to achieve enhanced barrier properties without impairing the mechanical performance.

Nanocellulose dispersion

The mechanical,[19] gas barrier,[18] and decomposition properties of the nanocomposites thus produced were expected to correlate strongly with the quality of nanocellulose dispersion in the polymer matrix. Hence, we characterized the size and distribution of (OLLA-g-)BC in the nanocomposites.

The improved dispersibility of OLLA-g-BC nanoparticles compared to unmodified BC nanoparticles in PLLA or PHBV was already evident in a visual inspection of the films (Fig. 4A and D). Millimeter-sized aggregates are visible for pure BC nanocomposites. Films produced with unmodified BC using
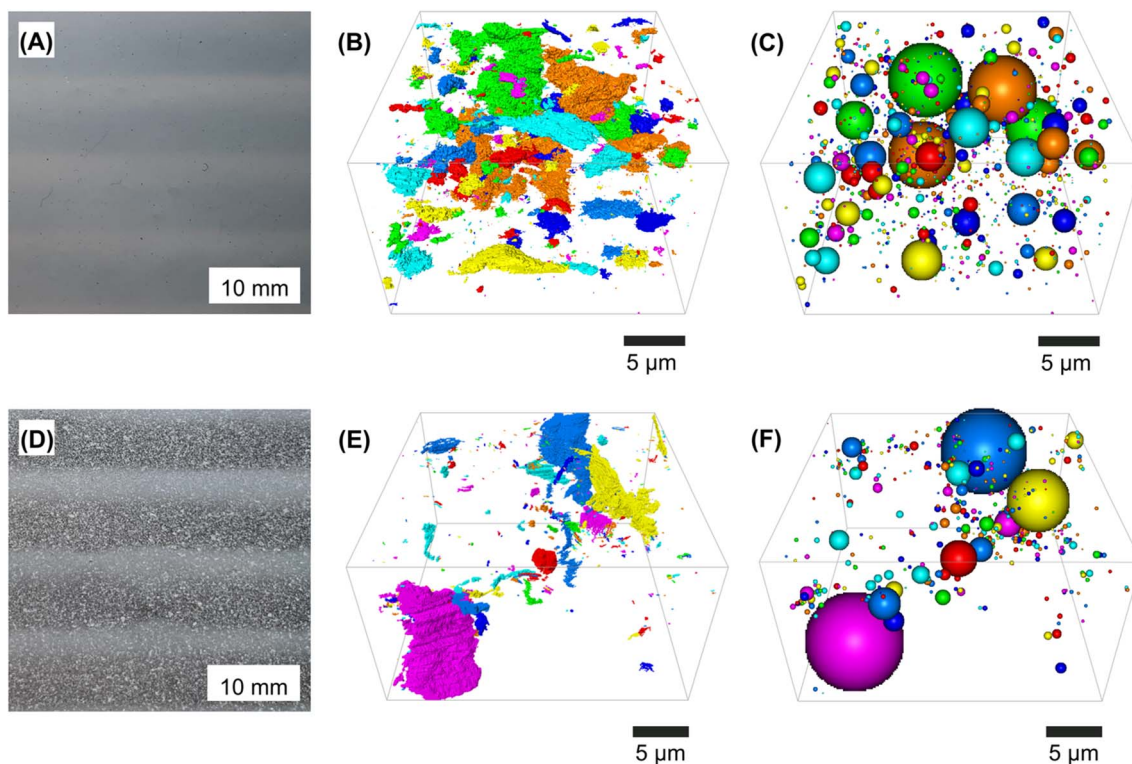

Fig. 4 Films produced by compression molding of (A) PLLA/OLLA-g-BC (5 wt%) and (D) PLLA/unmodified BC (5 wt%) (visual size images). 3D reconstructed SEM images of PLLA composites with (B) OLLA-g-BC and (E) unmodified BC particles. (C) and (F) Schematically show the equivalent volume of each aggregate as the volume of a sphere calculated with the program AMIRA™.

extrusion followed by compression molding at 180 °C were often discolored and variable in texture and thickness, while the OLLA-g-BC nanocomposites were homogeneous and optically transparent. The OLLA-g-BC nanocomposites displayed a rougher surface than the pure matrix polymer but no visible aggregates on cryogenic fracture surfaces (Fig. S2†).

We used serial block-face scanning electron microscopy (SBF-SEM) to visualize the 3D dispersion of BC nanoparticles in PLLA nanocomposites. The commercially available PHBV Enmat Y1000P contains boron nitride and antioxidant additives in the form of nanoparticles. We could not distinguish additive nanoparticles from the cellulose particles (Fig. S1 and S2D†). Therefore, our results are limited to PLLA nanocomposites, but we expect similar results for PHBV produced following the protocol for unmodified vs. OLLA-grafted BC nanoparticles.

For both PLLA nanocomposites, the scanning electron micrographs revealed an imperfect dispersion of two phases, corresponding to the continuous polymer matrix and the filler particles – OLLA-g-BC versus unmodified BC in Fig. 4B and E, respectively. In the 3D images, the colored areas represent the filler.

Our nanocomposites contained a filler volume fraction of 4.2 $\pm$ 0.9% according to density measurements (Table S1†). The volume fractions found by SBF-SEM were 1.8 $\pm$ 0.9% and 6 $\pm$ 1.9% for BC and OLLA-g-BC, respectively. The difference between nanocomposites containing unmodified BC, evident in Fig. 4D, and the volume fraction found using this method are explained by the limitations of SBF-SEM. This method could only produce an image of an area of 500–750 μm^2 of the nanocomposites with sufficient contrast between filler and matrix areas, which limited the volume we could observe. The higher-than-expected volume fraction of OLLA-g-BC filler material is mainly explained by the gaps between these particles in aggregates (Fig. 3D) or when they are unevenly distributed. Small gaps were not recognized by the SEM and the AMIRA™ software used to annotate the agglomerates, leading to a systematic overestimation of the volume fraction within observed sections.

Summarizing the optical and microscopic inspection, OLLA-grafting of BC suppressing macroscopic aggregation and improved its dispersibility. Although it does not guarantee perfect distribution of the nanoparticles within the matrix, the observed aggregates are micro- and nanoscale but small clusters were evenly distributed throughout the PLLA matrix. Hence, we limited materials testing to OLLA-g-BC nanocomposites and compared them to pure PLLA and PHBV. Unmodified BC nanocomposites did not display the optical properties and sample homogeneity required of packing materials.

Barrier properties of nanocomposites

One of the most essential properties of food packaging materials is the oxygen permeability (OP) and water vapor permeability (WVP). OP can be assessed by determining the oxygen transmission rate (OTR). WVP can be calculated from measured water vapor transmission rates (WVTR). The gas transmission rates of the nanocomposites were measured and compared to pure PLLA and PHBV in Fig. 5.
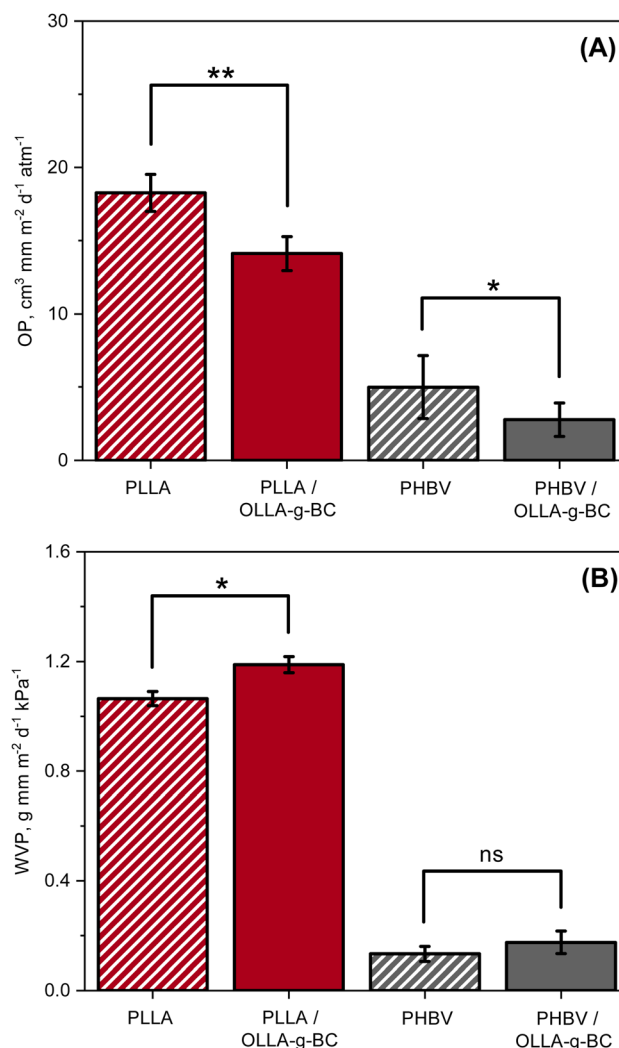

Fig. 5 Comparison of oxygen and water permeabilities: (A) oxygen and (B) water vapor permeability of PLLA, PLLA/OLLA-g-BC, PHBV, and PHBV/OLLA-g-BC.

The OP for PLLA was found to be 18.3 cm^3 mm m^{-2} d^{-1} atm^{-1}, and was reduced by $\sim$23% to 14.1 cm^3 mm m^{-2} d^{-1} atm^{-1} after adding 5 wt% of OLLA-g-BC nanofiller to the matrix. A similar effect was observed when incorporating of OLLA-g-BC into PHBV – the measured OP for pure matrix was found to be 5 cm^3 mm m^{-2} d^{-1} atm^{-1} and reduced by $\sim$45% to 2.8 cm^3 mm m^{-2} d^{-1} atm^{-1}. The reduction in OP could be attributed predominantly to the increased crystallinity of polymer matrix, from 6.2% to 12%, which was confirmed by the DSC for PLLA (Table S2†). However, the crystallinity of PHBV exhibited a slight decrease after adding OLLA-g-BC, from 52% to 50.1% (Table S2†), which leads us to assume that the diffusion of oxygen molecules was also reduced by the increased tortuous diffusion pathway for oxygen through the nanocomposite.[15]

The WVP for the PLLA nanocomposite slightly increased by $\sim$12% compared to pure PLLA, from 1.06 g mm m^{-2} d^{-1} kPa^{-1} to 1.19 g mm m^{-2} d^{-1} kPa^{-1}. A similar trend was observed for PHBV, for which WVP increased by $\sim$31% from 0.13 g mm m^{-2}

$d^{-1} kPa^{-1}$ for pure PHVB to 0.17 g mm m^{-2} d^{-1} kPa^{-1} for PHBV/OLLA-g-BC. However, the difference in WVP between PHBV and PHVB nanocomposite was statistically insignificant. The water permeability can increase because the presence of cellulose fillers contributes to water transport, which was confirmed by water uptake measurements (Fig. S3†). The addition of OLLA-g-BC to PLLA and PHBV increased the amount of sorbed water to 1.3 ± 0.1 wt% and 1.1 ± 0.3 wt% compared to 0.8 ± 0.1 wt% and 0.5 ± 0.1 wt% for the pure polymer matrices, respectively. WVTR was measured in accordance with standard GB/T 1037-1988 at 38 °C, which accelerates the hydrolysis of OLLA due to its temperature dependence,[57] causing structural defects in the polymer matrix and promoting water vapor penetration.

Mechanical properties of nanocomposites

The effect of OLLA-g-BC on the mechanical properties of PLLA and PHBV was investigated using tensile tests (Table 1). The effect of OLLA-g-BC nanofillers on the tensile modulus differed for the two polymer matrices. The Young's modulus of the PLLA nanocomposite increased by ~12%, whereas a 14% decrease in Young's modulus was observed for the PHBV nanocomposite. The observed changes in the Young's moduli of the nanocomposites correlate with the crystallinity of the polymer matrix (Table S2†). The slight decreases observed in tensile strengths of the nanocomposites were statistically insignificant, given the variability of the measurements.

Table 1 Mechanical properties of PLLA, PLLA/OLLA-g-BC, PHBV, and PHBV/OLLA-g-BC[a]

Sample	Tensile modulus (GPa)	Tensile strength (MPa)	Elongation at break (%)
PLLA	1.7 ± 0.2	61 ± 2.4	4.2 ± 0.3
PLLA/OLLA-g-BC	$1.9 \pm 0.1^*$	58 ± 2.4^{ns}	$3.7 \pm 0.3^*$
PHBV	2.2 ± 0.1	31 ± 3.2	1.9 ± 0.2
PHBV/OLLA-g-BC	$1.9 \pm 0.1^*$	28 ± 2.3^{ns}	$2.0 \pm 0.2^*$

[a] Statistical significance: "***": 0–0.001, "**": 0.001–0.01, "*": 0.01–0.05, "ns": 0.05–1.0. Statistical significance was evaluated for the differences between the pure polymers (PLLA or PHBV) and their respective composites.

Furthermore, the effect of filler was shown in the elongation at break for the PLLA nanocomposite, which slightly reduced, whereas PHBV/OLLA-g-BC did exhibit insignificant changes. The reduced elongation at break of the nanocomposites is commonly observed in thermoplastic composites in which the addition of stiff reinforcements causes stress concentrations.[14]

Biodegradation of nanocomposites

To evaluate the biodegradation of the filler and nanocomposites the CO_2 evolution of BC, OLLA-g-BC, PLLA and PLLA/OLLA-g-BC was measured (Fig. S4†). As expected, PLLA showed almost no biodegradation potential under environmental conditions[58] shown in Fig. 6A and a similar trend was observed for OLLA-g-BC in contrast to biodegradable BC. The decreased biodegradability of BC under mesophilic conditions after modification with oligolactic acid may indicate the formation of OLLA-g-BC core–shell particles for which the OLLA shell inhibits access of bacterial cellulases to the cellulose core. This interpretation is consistent with structural and grafting evaluations based on TGA and NMR data.

PLLA demonstrated biodegradability under thermophilic conditions (Fig. 6B) but is resistant to enzymatic attack, leading to very long biodegradation times (Fig. S5†). Nevertheless, OLLA-g-BC exhibited a similar biodegradability rate as cellulose at thermophilic conditions, which might be attributed to the temperature-accelerated hydrolysis of short-chain OLLA[57] with subsequent exposure of BC.

The biodegradation rate of PHBV nanocomposites has a predictable downward trend due to the similar behavior of OLLA and PLLA under mesophilic conditions and higher biodegradation rate of PHBV than cellulose and OLLA under thermophilic conditions.[59] Therefore, the influence of nanoparticles on the biodegradability of a polymer matrix was shown only for PLLA/OLLA-g-BC in an aquatic setup at thermophilic conditions (Fig. 6C). After the addition of OLLA-g-BC to PLLA, the nanocomposite showed a shorter lag phase and degraded faster than pure PLLA. This result may be attributed to the improved access of hydrolases to the material due to the increased surface roughness as shown by SEM (Fig. S2†). Furthermore, the addition of cellulose-based fillers decreased
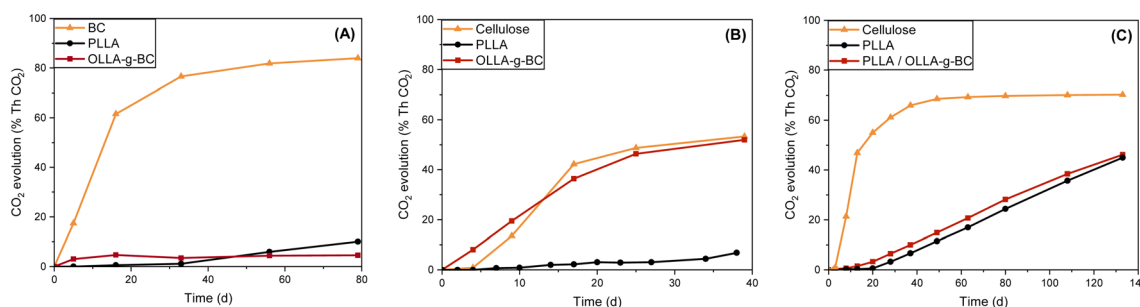

Fig. 6 CO_2 evolution of nanomaterials and pure PLLA in an aquatic test (A) under mesophilic (22 °C) aerobic conditions because of biodegradation by a mixed bacterial inoculum deriving from sewage sludge, (B) under thermophilic (58 °C) aerobic conditions because of biodegradation by a mixed bacterial inoculum deriving from biowaste compost. (C) CO_2 evolution of PLLA and PLLA/OLLA-g-BC in an aquatic test under thermophilic (58 °C) aerobic conditions as a result of biodegradation by a mixed bacterial inoculum deriving from biowaste compost. Cellulose (Fluka, Nr.: 22181) was used as reference material.

the hydrophobicity of the nanocomposite and consequently enhances the water and moisture absorption, which leads to a higher biodegradability rate of the polymer matrix.[15] In addition, the increased biodegradation rate of the nanocomposite might result from temperature-induced chemical hydrolysis of PLLA into oligomers, which are more available for bacterial hydrolases.

Conclusions

This study demonstrates that the simple grafting-from polymerization of OLLA onto the surface of nanoscale bacterial cellulose significantly enhances the dispersibility of the nanoparticles and improves the homogeneity of the resulting polymer blends. Incorporating 5 wt% OLLA-g-BC reduces oxygen permeability of PLLA and PHBV by approximately 23% and 45%, respectively. While the water permeability of PLLA increased by approximately 12%, the observed changes in PHBV were negligible. Enhancing the oxygen barrier aids in preventing oxidative spoilage, while regulating water vapor permeability mitigates food perishability and extends shelf life.[60] The introduction of filler had no significant impact on mechanical properties, resulting in only minor changes in the Young's moduli of the nanocomposites and a slight decrease in the elongation at break of PLLA.

By incorporating OLLA-g-BC into the polymers, the hydrolytic degradation rate of the nanocomposites was significantly increased under thermophilic conditions. The OLLA shell, which is responsible for the improved dispersibility, leads to greatly enhanced functional properties while hindering access to the filler during degradation processes. Despite the use of short-chain oligomers to achieve interfacial compatibility, the impact on degradation remains significant. An exciting area for further investigation could be if dispersibility and other properties could be improved by grafting shells with different polymer lengths, resulting in stronger repulsion between particles and more similar rheological properties to the bulk polymer.

In summary, combining efficient methods to modify pure as-produced bacterial cellulose with oligo-lactic acid and standard polymer processing methods to produce nanocomposites can result in low-cost and sustainable alternatives to conventional fossil-based plastics for the food packaging industry. We have already demonstrated that sufficient performance can be achieved using even an imperfect core–shell cellulose-based filler, indicating that the key to success is further improving the dispersibility of nano-sized bacterial cellulose core–shell nanoparticles.

Data availability

The data supporting this article have been included as part of the ESI.†

Conflicts of interest

There are no conflicts to declare.

Acknowledgements

References

1 G. Fackelmann, C. K. Pham, Y. Rodríguez, M. L. Mallory, J. F. Provencher, J. E. Baak and S. Sommer, *Nat. Ecol. Evol.*, 2023, **7**(5), 698–706.
2 M. I. Muhib, M. K. Uddin, M. M. Rahman and G. Malafaia, *Sci. Total Environ.*, 2023, **865**, 161274.
3 N. Jakrawatana, P. Ngammuangtueng, N. Vorayos and S. H. Gheewala, *Sustain. Prod. Consum.*, 2023, **39**, 506–520.
4 *Global Plastic Packaging Industry – Statistics & Facts | Statista*, https://www.statista.com/topics/10136/plastic-packaging-industry-worldwide/#dossier-chapter1, (accessed 19 July 2023).
5 *The Production of Plastic and Petrochemical Feedstocks*, https://revenuesandprofits.com/how-exxonmobil-makes-money/, (accessed 6 June 2024).
6 R. Muthuraj, M. Misra and A. K. Mohanty, *J. Appl. Polym. Sci.*, 2018, **135**, 45726.
7 P. Skoczinski, M. Carus, D. De Guzman, H. Käb, R. Chinthapalli, J. Ravenstijn, W. Baltus and A. Raschka, Bio-based building blocks and polymers-global capacities, production and trends 2020–2025, *Language*, 2021, 16.
8 *Biodegradability of Plastics in the Open Environment*, https://research-and-innovation.ec.europa.eu/strategy/support-policy-making/scientific-support-eu-policies/group-chief-scientific-advisors/biodegradability-plastics-open-environment_en, (accessed 11 June 2023).
9 *Communication from the Commission to the European Parliament, the European Economic and Social Committee and the Committee of the Regions. EU Policy Framework on Biobased, Biodegradable and Compostable Plastics*, https://eur-lex.europa.eu/legal-content/EN/TXT/PDF/?uri=CELEX:52022DC0682, (accessed 6 June 2024).
10 K. Madhavan Nampoothiri, N. R. Nair and R. P. John, *Bioresour. Technol.*, 2010, **101**, 8493–8501.
11 W. D. Luzier, *Proc. Natl. Acad. Sci. U. S. A.*, 1992, **89**, 839–842.
12 A. El-Hadi, R. Schnabel, E. Straube, G. Müller and S. Henning, *Polym. Test.*, 2002, **21**, 665–674.
13 N. Jabeen, I. Majid and G. A. Nayik, *Cogent Food Agric.*, 2015, **1**, 1117749.
14 K. Y. Lee, J. J. Blaker and A. Bismarck, *Compos. Sci. Technol.*, 2009, **69**, 2724–2733.
15 F. V. Ferreira, A. Dufresne, I. F. Pinheiro, D. H. S. Souza, R. F. Gouveia, L. H. I. Mei and L. M. F. Lona, *Eur. Polym. J.*, 2018, **108**, 274–285.
16 J. W. Rhim, S. I. Hong and C. S. Ha, *LWT–Food Sci. Technol.*, 2009, **42**, 612–617.
17 D. Plackett, T. L. Andersen, W. B. Pedersen and L. Nielsen, *Compos. Sci. Technol.*, 2003, **63**, 1287–1296.

18 C. Wolf, H. Angellier-Coussy, N. Gontard, F. Doghieri and V. Guillard, *J. Membr. Sci.*, 2018, **556**, 393–418.

19 Y. S. Song and J. R. Youn, *Carbon*, 2005, **43**, 1378–1385.

20 M. Dadras Chomachayi, P. Blanchet, A. Hussain and S. Pepin, *J. Polym. Environ.*, 2023, **31**, 5309–5325.

21 X. Li, J. Li, X. Shen, M. Cao, Y. Wang, W. Zhang, Y. Xu, Z. Ling, S. Chen and F. Xu, *ACS Sustain. Chem. Eng.*, 2024, **12**, 5427–5435.

22 L. Jiang, E. Morelius, J. Zhang, M. Wolcott and J. Holbery, *J. Compos. Mater.*, 2008, **42**, 2629–2645.

23 D. Bondeson and K. Oksman, *Compos. Interfaces*, 2007, **14**, 617–630.

24 M. Martínez-Sanz, A. Lopez-Rubio and J. M. Lagaron, *Biomacromolecules*, 2012, **13**, 3887–3899.

25 T. Lu, S. Liu, M. Jiang, X. Xu, Y. Wang, Z. Wang, J. Gou, D. Hui and Z. Zhou, *Composites, Part B*, 2014, **62**, 191–197.

26 D. Roy, M. Semsarilar, J. T. Guthrie and S. Perrier, *Chem. Soc. Rev.*, 2009, **38**, 2046–2064.

27 S. H. Osong, S. Norgren and P. Engstrand, *Cellulose*, 2015, **23**, 93–123.

28 S. O. Dima, D. M. Panaitescu, C. Orban, M. Ghiurea, S. M. Doncea, R. C. Fierascu, C. L. Nistor, E. Alexandrescu, C. A. Nicolae, B. Trica, A. Moraru and F. Oancea, *Polymers*, 2017, **9**, 374.

29 W. Czaja, D. Romanovicz and R. malcolm Brown, *Cellulose*, 2004, **11**(3), 403–411.

30 M. Iguchi, S. Yamanaka and A. Budhiono, *J. Mater. Sci.*, 2000, **35**, 261–270.

31 M. Jonoobi, R. Oladi, Y. Davoudpour, K. Oksman, A. Dufresne, Y. Hamzeh and R. Davoodi, *Cellulose*, 2015, **22**, 935–969.

32 A. Isogai and R. H. Atalla, *Cellulose*, 1998, **5**, 309–319.

33 A. P. Provin, A. Regina De Aguiar Dutra, I. C. Aguiar De Sousa, S. Gouveia, A. Leal and V. Cubas, *Technol. Forecast. Soc. Change*, 2021, **169**, 120858.

34 Y. Liu, Y. Zheng, T. Yang, J. Mac Regenstein and P. Zhou, *Trends Food Sci. Technol.*, 2022, **129**, 608–616.

35 *Kombucha Market Size, Share & Trends Report, 2022–2030*, https://www.grandviewresearch.com/industry-analysis/kombucha-market, (accessed 6 June 2024).

36 H. T. Nguyen and N. Saha, *Cellulose*, 2021, **28**, 9335–9353.

37 A. Gupta and V. Katiyar, *ACS Sustain. Chem. Eng.*, 2017, **5**, 6835–6844.

38 M. E. Genovese, L. Puccinelli, G. Mancini, R. Carzino, L. Goldoni, V. Castelvetro and A. Athanassiou, *ACS Sustain. Chem. Eng.*, 2022, **10**, 9401–9410.

39 S. Hua, F. Chen, Z. Y. Liu, W. Yang and M. B. Yang, *RSC Adv.*, 2016, **6**, 1973–1983.

40 R. Patwa, N. Saha, P. Sáha and V. Katiyar, *J. Appl. Polym. Sci.*, 2019, **136**, 47903.

41 J. Ambrosio-Martín, M. J. Fabra, A. Lopez-Rubio and J. M. Lagaron, *Cellulose*, 2015, **22**, 1201–1226.

42 H. Tan, H. Wang, Y. Tang, S. Zhang, W. Yang, Z. Liu and M. Yang, *Polym. Int.*, 2018, **67**, 1535–1544.

43 ISO, *ISO 527-2:2012 – Plastics — Determination of Tensile Properties — Part 2: Test Conditions for Moulding and Extrusion Plastics*, Geneva, 2012.

44 ASTM International, *D638 Standard Test Method for Tensile Properties of Plastics*, West Conshohocken, PA, 2022.

45 China National Standards, *Plastics–Film and Sheeting–Determination of Gas Transmission–Differential-Pressure Method*, Shenzhen, 2000.

46 China National Standards, *Test Method for Water Vapor Transmission of Plastic Film and Sheet–Cup Method*, Shenzhen, 1988.

47 CEN, *Packaging – Requirements for Packaging Recoverable through Composting and Biodegradation – Test Scheme and Evaluation Criteria for the Final Acceptance of Packaging*, Brussels, 2000.

48 OECD, Test No. 301: Ready Biodegradability, *OECD Guidelines for the Testing of Chemicals*, Paris, 1992.

49 İ. Bağlan, E. Yanbakan, T. Tuncel, A. Koçak Sezgin, E. Bozoğlan, D. Berikten and F. Kar, *J. Cell. Mol. Med.*, 2024, **28**, e18316.

50 Y. Luan, J. Wu, M. Zhan, J. Zhang, J. Zhang and J. He, *Cellulose*, 2013, **20**, 327–337.

51 S. Y. Oh, I. Y. Dong, Y. Shin, C. K. Hwan, Y. K. Hak, S. C. Yong, H. P. Won and H. Y. Ji, *Carbohydr. Res.*, 2005, **340**, 2376–2391.

52 C. Yan, J. Zhang, Y. Lv, J. Yu, J. Wu, J. Zhang and J. He, *Biomacromolecules*, 2009, **10**, 2013–2018.

53 E. Wojtczak, P. Kubisa and M. Bednarek, *Polym. Degrad. Stab.*, 2018, **151**, 100–104.

54 K. Y. Lee, G. Buldum, A. Mantalaris and A. Bismarck, *Macromol. Biosci.*, 2014, **14**, 10–32.

55 R. Jonas and F. Luiz, *Farah*, 1998, **59**, 101–106.

56 K. Oksman, A. P. Mathew, D. Bondeson and I. Kvien, *Compos. Sci. Technol.*, 2006, **66**, 2776–2784.

57 G. Schliecker, C. Schmidt, S. Fuchs and T. Kissel, *Biomaterials*, 2003, **24**, 3835–3844.

58 J. Muller, C. González-Martínez and A. Chiralt, *Materials*, 2017, **10**, 952.

59 S. Luo and A. N. Netravali, *Polym. Degrad. Stab.*, 2003, **80**, 59–66.

60 J. Zhou, X. Ma, J. Li and L. Zhu, *Cellulose*, 2019, **26**, 979–990.